PACS numbers: 81.05.Uw; 81.70.Fy; 78.20.Nv; 78.20.Ci; 42.70.Hi; 42.25.Bs
DOI: 10.1070/QE2008v038n12ABEH013822

Measurement of optical absorption in polycrystalline CVD diamond plates by the phase photothermal method at a wavelength of 10.6 μm

A.Yu. Luk'yanov, V.G. Ral'chenko, A.V. Khomich, E.V. Serdtsev, P.V. Volkov, A.V. Savel'ev, V.I. Konov

***Abstract*. A highly-efficient phase photothermal method is developed for quantitative measurements of the small optical absorption coefficient in thin plates made of highly transparent materials in which bulk losses significantly exceed surface losses. The bulk absorption coefficient at 10.6 μm is estimated in polycrystalline diamond plates grown from the vapour phase (a CVD diamond). The results are compared with those for natural and synthetic diamond single crystals and with the concentrations of nitrogen and hydrogen impurities. The absorption coefficient of the best samples of the CVD diamond did not exceed 0.06 cm^{-1}, which, taking into account the high thermal conductivity of the CVD diamond (1800 – 2200 W mK^{-1} at room temperature), makes this material attractive for fabricating output windows of high-power CO_2 lasers, especially for manufacturing large-size optics.**

Keywords: *polycrystalline diamond, optical absorption, photothermal method, CO_2 laser.*

1. Introduction

Diamond optics has aroused recent interest because it can be used in technological cw CO_2 lasers [1, 2], in output windows of super-high-power gyrotrons (to deliver millimetre radiation) [3], in IR imaging systems, including military applications [4], in Raman laser converters [5]. This interest is explained by the unique combination of optical, mechanical and thermal properties of diamond, which determine its advantages as an optical material, especially in the IR range. Because of the symmetry of the cubic atomic lattice, the intrinsic one-phonon absorption is absent in diamond, which makes it transparent in the broadest spectral region from 225 nm to radio waves for the band gap of 5.4 eV. The exception is the absorption bands in the region from 2.5 – 7.5 μm, caused by the two- and three-phonon absorption mechanisms [6].

Compared to zinc selenide, which is a conventional material for the CO_2-laser windows, the thermal conductivity of diamond is more than two orders of magnitude higher and the thermooptical coefficient and the thermal expansion coefficient are significantly lower (Table 1). Therefore, despite a much stronger absorption of diamond at a wavelength of 10.6 μm than that of ZnSe [$\alpha = (3.3 - 3.6) \times 10^{-2}$ cm^{-1} for natural type-IIa single crystals [7, 8], $\alpha_{ZnSe} = (5 - 6) \times 10^{-4}$ cm^{-1}], the unwanted thermal lens effect in the case of an output diamond window of a CO_2 laser proves to be approximately 200 times weaker than that in the case of ZnSe windows [1, 9]. In addition, because of the high strength of diamond windows, their thickness can be decreased down to 0.7 – 1 mm, while the typical thickness of ZnSe windows is 6 mm.

The resistance of diamond windows to laser radiation is rather high, which allows them to withstand the action of a radiation beam from a CO_2 laser with the power density of about 100 kW mm^{-2} [2]. The highest hardness and chemical inertness of diamond provide a high service reliability of diamond windows, which are resistant to scratches and dirt. In addition, diamond is radiation hard (i.e. low sensitive to the action of UV radiation of the discharge plasma in the

Table 1. Parameters of a polycrystalline CVD diamond and ZnSe at room temperature [1, 4, 5].

Sample	K/ W mK^{-1}	H/GPa	dn/dT (10^{-6} K^{-1})	e/MPa	h/mm	$\gamma/10^{-6}$ K^{-1}	n		α/cm^{-1}	ε(%)
							$\lambda = 0.63$ μm	$\lambda = 10.6$ μm	$\lambda = 10.6$ μm	
CVD diamond	2000	90	10	350 – 600	0.7 – 1.0	1	2.39	2.38	0.03 – 0.10	Unknown**
ZnSe	17	8	92 – 107	1.8	4 – 6	7.1	2.6	2.4	0.0005 – 0.0006*	0.04***

N o t e : K is the thermal conductivity; H is the hardness; dn/dT is the thermooptical coefficient; e is the bending strength; h is the typical window thickness; γ is the thermal expansion coefficient; n is the refractive index; α is the absorption coefficient; ε is the surface absorption coefficient; * the quantity obtained from calorimetric measurements (usually presented without separation into bulk and surface losses), for a high-quality material the bulk quantity is $\alpha = 0.00025 - 0.0003$ cm^{-1}; ** obviously absent; *** minimal value (strongly depends on the quality of surface treatment).

A.Yu. Luk'yanov, E.V. Serdtsev, P.V. Volkov Institute For Physics of Microstructures, Russian Academy of Sciences, P.B.-105, 603600 Nizhnii Novgorod, Russia;
e-mail: luk@imp.sci-nnov.ru, volkov@imp.sci-nnov.ru;
V.G. Ral'chenko, A.V. Savel'ev, V.I. Konov A.M. Prokhorov General Physics Institute, Russian Academy of Sciences, ul. Vavilova 38, 119991 Moscow, Russia;
e-mail: ralchenko@nsc.gpi.ru, vik@nsc.gpi.ru;
A.V. Khomich V.A. Kotel'nikov Institute of Radio Engineering and Electronics, Russian Academy of Sciences, pl. Vvedenskogo 1, 141190 Fryazino, Moscow region, Russia; e-mail: khomich@ms.ire.rssi.ru

Received 7 February 2008; revision received 5 April 2008
Kvantovaya Elektronika **38** (12) 1171 – 1178 (2008)
Translated by I.A. Ulitkin

laser cell), stable in the aggressive media (even in the hydrofluoric acid) and preserves its properties at elevated temperatures.

Probably, the first paper, in which attention was paid to diamond as a promising material for output windows of high-power CO_2 lasers, was the work of Douglas-Hamilton et al. published in 1974 [9]; the paper reported the results of radiation resistance tests with a synthetic single crystal diamond of size $1 \times 2 \times 4$ mm irradiated by a cw 10-kW laser beam. Unfortunately, neither natural diamonds nor single crystals obtained by the conventional technology of synthesis at high temperatures cannot be used in practice in high-power lasers due to the limitation in their size (as a rule, it is several millimetres across). At the same time, modern methods for growing diamond films and plates from the vapour phase [the Chemical Vapour Deposition (CVD) technology] allow one to obtain optical-quality polycrystalline diamond plates of diameter more than 150 mm and thickness of more than 2 mm [10–12], whose properties can be close to those of especially pure diamond single crystals. The minimal absorption coefficients α of the CVD diamond measured at 10.6 μm are $0.030-0.065$ cm^{-1} [2, 13, 14]. Note that the absorption coefficient in the CVD diamond depends on the conditions of its synthesis affecting the concentration of defects and impurities; therefore, the precise control of this parameter, which is critical for producing IR optics, is very important.

At present, the most widely used method for measuring the absorption coefficient is the calorimetric method whose main advantage is the simplicity of realisation. However, interpretation of the data obtained by this method encounters substantial difficulties especially in those cases when it is necessary to study samples of different shapes, to determine separately the coefficients of bulk and surface absorption as well as to study their distribution in the sample [15, 16]. Concerning the CVD diamond, calorimetric measurements were performed in papers [2, 13, 14].

The mentioned problems can be overcome by using the thermal-wave diagnostic techniques, which are based on the measurement of a small periodic increase in the sample temperature caused by the absorption of time-modulated optical radiation [17, 18]. The thermal-wave methods also include the photoacoustic techniques for detecting thermal oscillations appearing upon periodic heating of the sample and its following expansion. The disadvantages of the photoacoustic techniques consist in the fact that it is not completely contactless (the samples should be fixed to a piezoelectric element or a cell with a microphone), which leads to poor reproducibility of the experimental data under special conditions: at high (low) temperatures or pressure, in a chemically active medium, etc.

Of special interest are photothermal spectroscopy optical methods because they are completely contactless, highly sensitive and have a large spatial resolution. Among these methods, the phase (interference) method [19–21], in which the change in the optical path length of the probe beam propagated through a heated region is measured with a probe interferometer, has the highest sensitivity. Application of different optical interferometers for detecting thermal waves has been described elsewhere [22–24]. Polarisation interferometers are especially convenient [24]. Their advantages include high stability and sensitivity and small overall dimensions. We have successively used such interferometers for photothermal detection of impurities in a highly-efficient liquid chromatography, for studying excited states in active crystals of Nd:YAG lasers and the electrooptic effect in polymers [25–27].

This work is devoted to the photothermal study of absorption in polycrystalline CVD diamond plates at a wavelength of 10.6 μm. We have shown that the growth technologies of this material available in Russia allow one to start in the near future the practical development of power diamond optics.

2. Samples

Transparent polycrystalline diamond films of thickness 0.3–0.5 mm were grown at the General Physics Institute of the Russian Academy of Sciences on silicon substrates of diameter 57 mm in the microwave plasma in CH_4/H_2 gas mixtures by using a special 5-kW, 2.45-GHz microwave UPSA-100 plasmochemical reactor [12]. Typical synthesis conditions were as follows: the methane concentration in the mixture was 0.9 %–2.5 %, the gas flow rate was 1.0 L min^{-1}, the pressure in the chamber was 90–95 Torr and the substrate temperature was 820–840 °C.

The diamond film structure was inhomogeneous – the lateral size of columnar crystallites was 50–80 μm on the growth side (Fig. 1) and ~ 1 μm on the side adjacent to the substrate. After chemical removal of the silicon substrate, the most defective 15–30-μm-thick diamond layer located on the small-grain side was abrasively polished. After laser cutting the initial diamond disk into plates of size no more than 8×8 mm, they were polished from both sides (Fig. 2) which provided the root-mean-square roughness $R_{rms} \sim 7-15$ nm (within one grain the roughness could be only 0.2 nm; however, at the grain boundaries there were 'steps' of height of several nanometers) [28]. The Raman spectra of all the samples under study exhibited only one strong and narrow (the FWHM is no more than 3 cm^{-1}) line at the 1332-cm^{-1} frequency, which is typical of a high-quality diamond. We failed to find the presence of non-diamond phases – amorphous carbon or graphite.

We compared two samples of the single crystalline diamond: colourless natural diamond close to the IIa type with a small content of nitrogen impurities (sample T-111) and yellowish synthetic (100)-cut diamond with a high concentration of nitrogen (grown in a high-pressure apparatus, sample MM). The facets of both single crystals

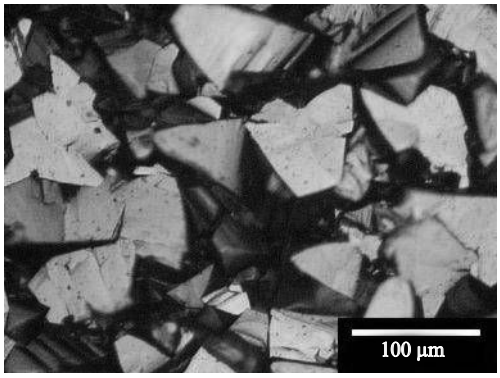

Figure 1. Unpolished surface of the polycrystalline diamond (sample 0905, optical microscope photography).

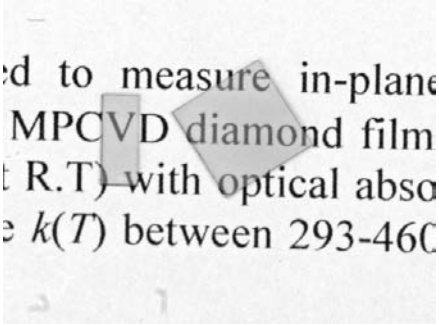

Figure 2. Polished CVD-diamond plates of size 8×8 and 3×7 mm.

were thoroughly polished. Some parameters of the samples under study are presented below in Table 2.

Absolute concentrations of hydrogen impurities (in the form of CH, CH_2 and CH_3 groups) and nitrogen impurities in the substituting site in the lattice node (C centre) in the CVD-diamond samples were determined from the optical transmission spectra $T(\lambda)$ in the UV (270 nm) and IR (2800 – 3100 cm^{-1}) regions by the method [29] involving Specord M400 and M80 (Carl Zeiss) spectrometers, respectively. In the IR spectral range, the photometric accuracy was $0.002T$. The concentration of nitrogen and hydrogen atoms was $(0.2 - 0.3) \times 10^{18}$ cm^{-3} and $(10 - 18) \times 10^{18}$ cm^{-3}, respectively.

We determined the nitrogen concentration and state in natural and synthetic crystals by analysing the shape of the IR absorption band in the one-phonon region (1400 – 800 cm^{-1}) [30] and the absorption spectra in the UV region in accordance with the calibration ratio from [31]. The band at 1280 cm^{-1} with the amplitude of about 1.4 cm^{-1} prevailed in the IR spectra of natural diamond. Natural diamond under study belongs to the IaB type [31]. The nitrogen concentration in the form of A centres (two nitrogen atoms in adjacent lattice nodes) was about 8×10^{18} cm^{-3}, the concentrations in the form of B1 and B2 centres [nitrogen segregations in (111) and (100) planes] were significantly lower. The absorption at the wavelength of 10.6 μm (945 cm^{-1}) in diamonds, where A centres prevail, was approximately 30 times smaller than that in the maximum at the frequency 1280 cm^{-1}, i.e. was 0.04 cm^{-1}.

The nonuniform colouring of the synthetic diamond single crystal is caused, first of all, by the inhomogeneous distribution of C centres in the growth sectors. According to the data on UV absorption (band at 270 nm) the nitrogen concentration in the substitution state changes in the sample from 5 to 30 ppm, i.e. within $(1 - 5) \times 10^{18}$ cm^{-3}. The one-phonon absorption spectra exhibit a complicated band with the maximum at 1280 cm^{-1}. In addition, the absorption bands are resolved at 1430 and 1350 cm^{-1}, a broad band with the maximum at 1170 – 1200 cm^{-1} and a band at 880 cm^{-1}, which also indicates the presence of A and B centres. According to the IR spectroscopy data, in the more coloured part of the sample the nitrogen concentration in the form of A centres is 100 ppm, B centres – 50 ppm, and C centres – 30 ppm. In its transparent part the nitrogen concentration is lower: 60 ppm in the form of A centres, 20 ppm – B centres, and 5 – 10 ppm in the form of C centres. The band in the IR spectra with the maximum at 880 cm^{-1} is most likely of the dislocation character because it is usually observed in plastically deformed synthetic and natural diamonds [32]. Hydrogen was not found in single-crystal samples.

Figure 3 presents the absorption spectra in the range from 175 nm to 20 μm for one of the CVD diamonds (0206) and for natural and synthetic single crystals. The transmission of the CVD diamond at 10.6 μm is close to the theoretical value 71.5 %, but in the UV region the polycrystalline diamond demonstrates higher losses both due to absorption and the increase in scattering supposedly at the grain boundaries. The band at 2.5 – 6.2 μm is caused by the multiphonon absorption [6].

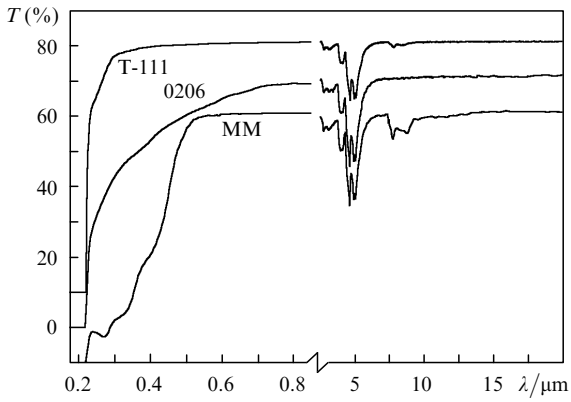

Figure 3. Transmission spectra of natural (T-111, displaced to the top by 10 % along the ordinate) and synthetic (MM, displaced to the bottom by 10 %) diamonds and a CVD diamond (0206).

3. Measurement technique

Figure 4 shows the scheme of the setup intended for quantitative measurements of absorption. The plate under study was placed in the probe interferometer perpendicular to probe beams (the probe radiation wavelength was 0.66 μm and the distance between the beam axes was 1 mm). By using a lens with the focal distance $F = 120$ mm, the pump radiation of cw CO_2 laser (LG-25, the power after propagation through the sample – 2.6 W) was focused into the waist region of one of the probe beams. The heating-beam radius was $r_0 = 220$ μm and the probe-beam radius was $\omega_0 = 60$ μm. The second probe beam propagated through the unheated region of the sample. The intersection regions of the probe and heating light beams with respect to the sample were scanned by displacing the latter along the propagation direction of probe beams (shown by the arrow in Fig. 4). In this case, the intersection region of the probe and heating light beams fell sequentially in air in front of the sample, on the front face, in the sample bulk, on the rear face and in air behind the sample. This method was user earlier to study optical absorption in ZnSe, ZnS and on thier antireflection coatings [33 – 36]. The CO_2-laser intensity at 6.7 kHz was modulated with the help of a mechanic chopper. The absorption of the CO_2-laser energy by the sample lead to the local variable (at the modulation frequency) heating and to the related changes in the refractive index, which, in turn, caused the change in the phase difference between the probe beams detected by the probe interferometer. The heating laser power (with the instability within 10 %) was continuously measured and the signal was normalised to it.

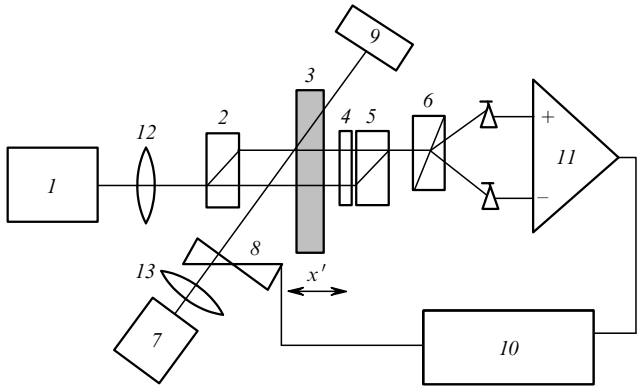

Figure 4. Scheme of the experimental setup: (*1*) probe diode laser ($\lambda = 0.66$ μm); (*2*, *5*) polarisation beamsplitters; (*3*) sample; (*4*) 90° optical rotator; (*6*) Wollaston prism; (*7*) heating CO_2 laser; (*8*) chopper; (*9*) power meter; (*10*) synchronous detector; (*11*) differential amplifier; (*12*, *13*) focusing lenses.

4. Theoretical description

Figure 5 presents the typical experimental dependence of the photothermal signal amplitude on the position of the intersection region of the probe and heating light beams with respect to the sample.

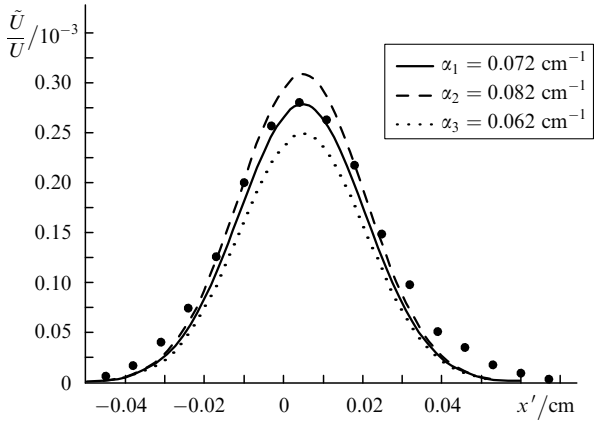

Figure 5. Theoretical (curves) and experimental (points) dependences of the measured photothermal signal U/U on the position x' of the intersection region of the probe and heating light beams for sample 0206; $f = 6.7$ kHz, $\omega_0 = 60$ μm, $r_0 = 220$ μm.

The spatial resolution 'across' the sample of thickness d is determined by the size of the heated region, i.e. the diameter D of the heating beam and the thermal diffusion length $\mu = [K/(C\rho 2\pi f)]^{1/2}$. Hereafter, K is the thermal conductivity coefficient, C is the heat capacity, ρ is the density and f is the modulation frequency. In the case under study ($d = 125 - 450$ μm, $D = 2r_0\sqrt{2} = 620$ μm due to the oblique incidence of the heating beam on the sample, $\mu = 170$ μm), $D + 2\mu > d$. As is expected, the shape of the photothermal response is close to the shape of the beam of the heating laser radiation, which size determines the spatial resolution. In this case, it is insufficient for studying the absorption distribution over the sample thickness, therefore, we assume that the heat is released uniformly only in the sample bulk. This assumption should be fulfilled with a high probability because due to the large enough coefficient of bulk absorption in diamond, the surface absorption in the form observed in ZnSe [33–35] is obviously absent, which is indirectly confirmed by the results of Ref. [14].

Thus, to describe the detected signal, we consider the sample of thickness d with the coefficient of bulk absorption α, which is in contact with nonabsorbing air (Fig. 6). In this case, the amplitude of the photothermal response will be proportional to the total absorption in the sample. In addition, we assume in the theoretical description that the intersection region of the probe and heating light beams was scanned not by displacing the latter along the probe beams by the quantity x' (Fig. 5) but by displacing the probe beams along the sample by the quantity x_0 (Fig. 6). To relate these displacements, we will use Fig. 7, which gives

$$\tan\theta_1 = \frac{\Delta + x_0}{x'},$$

$$\tan\theta_2 = \frac{\Delta}{x'},$$

which yields $x_0 = x'(\tan\theta_1 - \tan\theta_2)$.

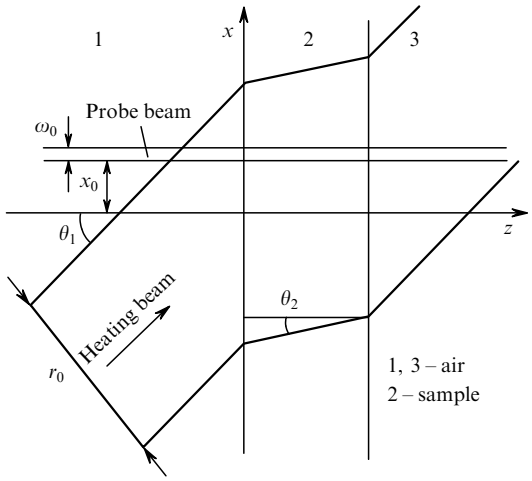

Figure 6. Problem configuration (see the text).

We are interested in the temperature perturbation appearing due to absorption of heating radiation, which has a Gaussian intensity distribution $I(x, y, z, t)$ and attenuates during the propagation in the sample. The time dependence of the heating radiation intensity had a meander shape obtained with the help of the mechanic chopper:

$$I_i(x,y,z,t) = \frac{2}{\pi}\frac{P_i\cos\theta_1}{r_0^2}\exp\left[-\frac{2(x - z\tan\theta_i)^2}{r_0^2/\cos^2\theta_1} - \frac{2y^2}{r_0^2}\right] \times\left[1 + \sum_{m=1,3,5} a_m\sin(m\Omega t)\right]. \quad (1)$$

Hereafter, $i = 1, 2, 3$ corresponds to the number of the region under study (1, 3 – air, 2 – diamond); θ_1 in region 1 is the angle of radiation incidence on the sample; θ_2 in region 2 is the refraction angle; $\theta_3 = \theta_1$ is the refraction angle in region 3; r_0 is the pump beam radius; P_i is the

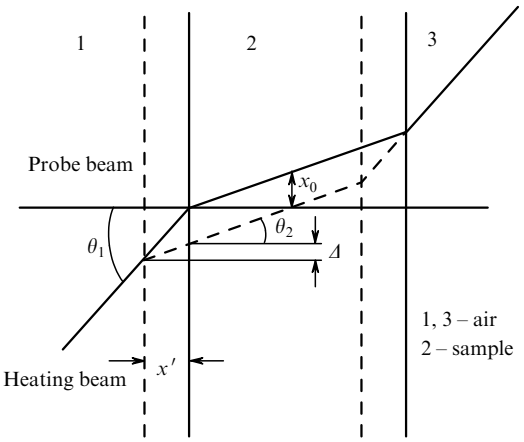

Figure 7. Displacement of the sample along the probe beam by the quantity x', equivalent to the displacement of the probe beam along the sample by the quantity x_0.

mean power of heating radiation in the ith region; $\Omega = 2\pi f$ is the circular frequency; $a_m = 4/\pi m$ is the amplitude of odd ($m = 1, 3, 5$) harmonics.

In this case, the thermal diffusion equation for each of the Fourier components of the required perturbations is:

$$\frac{\partial^2 T_m}{\partial x^2} + \frac{\partial^2 T_m}{\partial y^2} + \frac{\partial^2 T_m}{\partial z^2} - \frac{1}{\chi_i}\frac{\partial^2 T_m}{\partial x^2} = \frac{\alpha_i}{K_i} I_i(x, y, z) a_m \mathrm{Im}[\exp(\mathrm{i}m\Omega t)], \tag{2}$$

where K_i is the thermal conductivity coefficient; $\chi_i = K_i/\rho_i C_i$ is the thermal diffusivity; ρ_i is the density; and C_i is the heat capacity.

The temperature distribution $T_m(x, y, z, t)$ can be found in the form:

$$T_m(x, y, z, t) = \mathrm{Im}\left(\frac{\exp(\mathrm{i}m\Omega t)}{4\pi^2} \int_{-\infty}^{+\infty}\int_{-\infty}^{+\infty} \tilde{T}_m(\lambda, \delta, z) \times \exp(\mathrm{i}\lambda x + \mathrm{i}\delta y)\mathrm{d}\lambda\mathrm{d}\delta \right), \tag{3}$$

where $\tilde{T}_m(\lambda, \delta, z)$ is the amplitude of the mth harmonic.

Expression (2) for it can be written in the form:

$$\frac{\mathrm{d}^2 \tilde{T}_m(\lambda, \delta, z)}{\mathrm{d}z^2} - \xi_i^2 \tilde{T}_m(\lambda, \delta, z) = \frac{\alpha_i a_m P_i}{K_i} \times \exp\left(-\frac{r_0^2 \delta^2}{8} - \frac{r_0^2 \lambda^2 / \cos^2\theta_1}{8} \right) \exp(-\mathrm{i}z\lambda \tan\theta_2), \tag{4}$$

where

$$\xi_i = \left(\lambda^2 + \delta^2 + \frac{\mathrm{i}m\Omega}{\chi_i} \right)^{1/2}. \tag{5}$$

Taking into account that for the specified parameters ($f = 6.7$ kHz, $r_0 = 220$ μm, $K_1 = 2.5 \times 10^{-4}$ W cm^{-1}K^{-1}, $C_1 = 1$ J g^{-1} K^{-1}, $\rho_1 = 1.3 \times 10^{-3}$ g cm^{-3}, $K_2 = 22$ W cm^{-1} K^{-1}, $C_2 = 0.52$ J g^{-1} K^{-1}, $\rho_2 = 3.51$ g cm^{-3}) $\Omega/\chi_{1,2}$ is larger than λ^2 and δ^2, expression (5) can be approximately written in the form: $\xi_{1,2}^2 = \mathrm{i}m\Omega/\chi_{1,2}$.

By neglecting absorption in air ($\alpha_1, \alpha_3 \ll \alpha_2 = \alpha$) and taking into account the infinite increase in temperature when z tends to $\pm\infty$, we obtain solution (4) in regions 1, 2 and 3, respectively:

$$\tilde{T}_{m1}(\lambda, \delta, z) = A\exp(\xi_1 z), \tag{6}$$

$$\tilde{T}_{m2}(\lambda, \delta, z) = B\exp(-\xi_2 z) + a_m \frac{\alpha}{K_2}\frac{P_2}{\xi_2^2} \times \exp\left[-\frac{r_0^2}{8}\left(\frac{\lambda^2}{\cos^2\theta_1} + \delta^2 \right) - \mathrm{i}z\lambda\tan\theta_2 \right] + C\exp(\xi_2 z), \tag{7}$$

$$\tilde{T}_{m3}(\lambda, \delta, z) = D\exp(-\xi_1 z), \tag{8}$$

where A, B, C, and D are the constant coefficients determined from boundary conditions for $z = 0$ and $z = d$:

$$\begin{aligned} &\tilde{T}_{m1}(\lambda, \delta, z) = \tilde{T}_{m2}(\lambda, \delta, z)|_{z=0}, \\ &K_1 \frac{\mathrm{d}\tilde{T}_{m1}}{\mathrm{d}z} = K_2 \frac{\mathrm{d}\tilde{T}_{m2}}{\mathrm{d}z}|_{z=0}, \\ &\tilde{T}_{m2}(\lambda, \delta, z) = \tilde{T}_{m3}(\lambda, \delta, z)|_{z=d}, \\ &K_2 \frac{\mathrm{d}\tilde{T}_{m2}}{\mathrm{d}z} = K_1 \frac{\mathrm{d}\tilde{T}_{m3}}{\mathrm{d}z}|_{z=d}. \end{aligned} \tag{9}$$

Then,

$$A = \frac{2\exp(-\xi_1 d)F}{\Delta}\left[K_1\xi_1 K_2\xi_2 \cosh(\xi_2 d) + (K_2\xi_2)^2 \sinh(\xi_2 d) - K_1\xi_1 K_2 Q\sinh(\xi_2 d) - K_2^2\xi_2 Q\cosh(\xi_2 d) + 2K_2\xi_2\exp(-Qd)(K_2 Q - K_1\xi_1)\right], \tag{10}$$

$$B = \frac{\exp(-\xi_1 d)F}{\Delta}\left\{ -\exp(\xi_2 d)\left[(K_1\xi_1)^2 + K_1\xi_1 K_2\xi_2 + \xi_1 K_1 K_2 Q + \xi_2 K_2^2 Q \right] + \exp(-Qd) \times \left[(K_1\xi_1)^2 - K_1\xi_1 K_2\xi_2 - \xi_1 K_1 K_2 Q + \xi_2 K_2^2 Q \right] \right\}, \tag{11}$$

$$C = \frac{\exp(-\xi_1 d)}{\Delta}\left\{ \exp(-\xi_2 d)\left[(K_1\xi_1)^2 - K_1\xi_1 K_2\xi_2 + \xi_1 K_1 K_2 Q - \xi_2 K_2^2 Q \right] - \exp(-Qd)\times \times \left[(K_1\xi_1)^2 + K_1\xi_1 K_2\xi_2 - \xi_1 K_1 K_2 Q - \xi_2 K_2^2 Q \right] \right\}, \tag{12}$$

$$D = \frac{2F}{\Delta}\left\{ -K_1\xi_1 K_2\xi_2 + QK_2^2\xi_2 + \exp(-Qd)\times \times \left[K_1\xi_1 K_2\xi_2\cosh(\xi_2 d) + (K_2\xi_2)^2\sinh(\xi_2 d) \right] + Q\exp(-Qd)\left[K_1\xi_1 K_2\sinh(\xi_2 d) + K_2^2\xi_2\cosh(\xi_2 d) \right] \right\}, \tag{13}$$

where

$$F = a_m \frac{\alpha}{K_2} \frac{P_2}{\xi_2^2} \exp\left[-\frac{r_0^2}{8}\left(\frac{\lambda^2}{\cos^2\theta_1} + \delta^2\right)\right];$$

$$Q = \mathrm{i}\lambda \tan\theta_2;$$

$$\Delta = 2\exp(-\xi_1 d)\left[(K_2\xi_2)^2 \sinh(\xi_2 d) + (K_1\xi_1)^2 \sinh(\xi_2 d) + 2K_1\xi_1 K_2\xi_2 \cosh(\xi_2 d)\right].$$

The probe light at the wavelength λ_{prob}, which propagated through the region heated in this way perpendicularly to the interface, will acquire an additional phase incursion (under condition that the temperature perturbation and its gradient are rather small):

$$\tilde{\Phi}_m(\lambda, \delta) = \frac{2\pi}{\lambda_{\mathrm{prob}}} \frac{\partial n}{\partial T} \int_{-\infty}^{+\infty} \tilde{T}_m(\lambda, \delta, z)\mathrm{d}z. \quad (14)$$

A periodic change in the phase difference of the probe beams leads to periodic variations in the interference pattern at the probe interferometer output. By assuming the probe beam profile in the region of the temperature perturbation to be constant, the complex relative amplitude of these intensity variations at the frequency $2\pi fm$ detected by the far-field photodetector can be written by returning to the variables x and y [20, 21] in the form:

$$\frac{\Delta I_m}{I} = \int_{-\infty}^{+\infty}\int_{-\infty}^{+\infty} \mathrm{d}y |I_0(x, y)|^2 \tilde{\Phi}_m(x, y). \quad (15)$$

Here

$$|I_0(x, y)|^2 = \frac{2}{\pi\omega_0^2} \exp\left[-2\,\frac{(x - x_0)^2 + y^2}{\omega_0^2}\right] \quad (16)$$

is the intensity distribution of probe radiation in the heated region;

$$\tilde{\Phi}_m(x, y) = \frac{1}{4\pi^2} \int_{-\infty}^{+\infty}\int_{-\infty}^{+\infty} \tilde{\Phi}_m(\lambda, \delta) \exp(\mathrm{i}\lambda x + \mathrm{i}\delta y)\mathrm{d}\lambda\mathrm{d}\delta. \quad (17)$$

Solution (15) contains rather many terms of complex form. However, estimates showed that for the specified parameters the terms in the form

$$\frac{\Delta I_m}{I} = \frac{a_m}{m}\,\alpha\, \frac{2}{\lambda_{\mathrm{prob}} \tan\theta_2 \left(\omega_0^2 + r_0^2\right)^{1/2}} \sqrt{\frac{\pi}{2}} \left(\frac{\partial n}{\partial T}\right)_2 \frac{P_2}{\Omega\rho_2 C_2} \times \left\{\mathrm{erf}\left[\frac{\sqrt{2}(d\tan\theta_2 - x_0)}{\left(\omega_0^2 + r_0^2/\cos^2\theta_1\right)^{1/2}}\right] + \mathrm{erf}\left[\frac{\sqrt{2}\,x_0}{\left(\omega_0^2 + r_0^2/\cos^2\theta_1\right)^{1/2}}\right]\right\} \quad (18)$$

make the main contribution to the relative amplitude of the photothermal signal at the frequency $2\pi fm$.

Because the greater part of the signal energy is concentrated in the first harmonic, to improve the signal-to-noise ratio it is expedient to detect only it by transmitting the signal through the strip filter at the input of the synchronous detector. Taking into account that the synchronous detector measures the effective amplitude of the first harmonic, the detected relative voltage is finally obtained in the from

$$\frac{\tilde{U}}{U} = \frac{8}{\sqrt{\pi}}\, \frac{\alpha}{\lambda_{\mathrm{prob}} \tan\theta_2 \left(\omega_0^2 + r_0^2\right)^{1/2}} \left(\frac{\partial n}{\partial T}\right)_2 \frac{P}{\Omega\rho_2 C_2} \times \left\{\mathrm{erf}\left[\frac{\sqrt{2}(d\tan\theta_2 - x_0)}{\left(\omega_0^2 + r_0^2/\cos^2\theta_1\right)^{1/2}}\right] + \mathrm{erf}\left[\frac{\sqrt{2}\,x_0}{\left(\omega_0^2 + r_0^2/\cos^2\theta_1\right)^{1/2}}\right]\right\},$$

where U is the half the amplitude of the constant voltage at the output of the differential amplifier when the phase difference of the probe beams changes by 2π.

5. Discussion of results

Figure 5 presents theoretical and experimental dependences of the relative amplitude $\tilde{U}/U$ of the photothermal signal on the position of the intersection point of the heating and probe light beams for sample 0206.

The theoretical profiles were obtained for three different values of the absorption coefficient α. One can see that the best coincidence with the measurements corresponds to $\alpha = 0.072\ \mathrm{cm}^{-1}$.

For all samples we observed some discrepancy of experimental points with experimental dependences, mainly in the distribution wings. This is caused by the fact that in the theoretical description we assumed the thermal diffusion length to be much smaller that the heating beam radius, which is not quite true. We can estimate the observed discrepancy by calculating the areas below the experimental and theoretical curves; the difference between these areas is 1.1 times. Thus, the absorption coefficient should be increased by 1.1 times, which, however, does not exceed the accuracy of the experiment (±20 %). The noise level in the measurements corresponds to the absorption coefficient, which is no higher than $10^{-2}\ \mathrm{cm}^{-1}$.

The measured optical absorption coefficients of diamond plates are presented in Table 2. Three CVD-diamond samples out of four under study have the coefficient $\alpha < 0.08\ \mathrm{cm}^{-1}$ and its minimal value is $0.057\ \mathrm{cm}^{-1}$. The

Table 2. Parameters of natural (T-111) and synthetic (MM) diamond samples and of four CVD-diamond samples studied in this paper.

Sample	Sample dimensions/mm	$N_{\mathrm{N}}/10^{18}$ cm^{-3}	$N_{\mathrm{H}}/10^{18}$ cm^{-3}	α/cm^{-1}	α_{t}/cm^{-1}
0206	8 × 8 × 0.31	0.2	13.5	0.079	0.09 ± 0.05
BKP-2	8 × 8 × 0.23	0.2	18.0	0.12	0.14 ± 0.05
0905	7 × 3 × 0.45	0.3	11.5	0.06	0.08 ± 0.04
1005	8 × 8 × 0.45	0.2	10.0	0.057	0.08 ± 0.04
MM	∅3.3 × 0.32	15	–	0.086*	0.2
		–		0.345*	–
		32		0.53*	0.5
T-111	4 × 3 × 0.18	6	–	0.086	0.08 ± 0.05

N o t e . The concentrations N of impurity nitrogen and hydrogen atoms are given. The absorption coefficients at 10.6 μm are measured by the photothermal method (α) and obtained from the transmission spectra (α_{t}).
* Local values in the synthetic single crystal in three regions with different content of nitrogen impurities (optical transmission spectra were measured in regions of size 1 × 1 mm).

absorption increases with increasing the content of hydrogen impurities, which is not strange because hydrogen has a tendency to decorate defects in diamond and is a good defectiveness indicator of the material [37]. Note that according to data from paper [38] the integral (over angles) quantity of the optical scattering from defects and grain boundaries in the polycrystalline CVD diamond is two orders of magnitude higher than in single crystals, but does not exceed 1 %.

In most perfect diamond single crystals the absorption coefficient at 10.6 μm is 0.033 – 0.036 cm^{-1} [7, 8]. This is the lowest threshold caused by the long wavelength 'tail' of the two-phonon absorption band in the region from 3.75 – 7.5 μm [6]. In the synthetic single crystal (sample MM) the absorption coefficient is several times higher (0.086 – 0.53 cm^{-1}), which is explained by the increased (by two orders of magnitude compared to the CVD diamond) content of nitrogen. The difference in the absorption coefficients within one sample is explained by the known phenomenon of inhomogeneous distribution of impurity nitrogen atoms in the growth sectors [39]. This distribution leads to the nonuniform colouring of the crystal in the visible spectrum (from colourless to yellow). Thus, the possibility of the local probing of even small objects by the photothermal method has been demonstrated. In this case, the spatial resolution was about 0.8 mm, but it can be easily improved several times by increasing the modulation frequency and decreasing the diameter of the heating beam.

The data on absorption (α_t) obtained from the transmission spectra at 10.6 μm, on the whole, well agree with the quantities determined by the photothermal method; however, the error in determining α_t for the most transparent samples is much higher – of the order of 50 %.

For polycrystalline diamond sample 0905, the measurements of the thermal conductivity coefficients along the plate ($K_\parallel$) and along the normal to it ($K_\perp$) yielded $K_\parallel = 1820$ W mK^{-1} and $K_\perp = 2280 + 170$ W mK^{-1} [40], which are close to the thermal conductivity coefficients of type IIa single crystals. The anisotropy of thermal conductivity (about 20 %) is caused by the peculiarities of the crystallite structure, namely, by a higher frequency of phonon scattering at the grain boundaries during the propagation of phonons across column crystallites ($K_\parallel$) compared to the direction along the columns ($K_\perp$). Such large thermal conductivity coefficients justify the selection of the polycrystalline diamond as a material for power optics in the IR range.

6. Conclusions

By using the phase photothermal method, we have measured the bulk absorption at a wavelength of 10.6 μm in plates made of the polycrystalline CVD diamond grown in the microwave plasma and in samples from natural and synthetic diamond single crystals. The method allows the local probing with the resolution less than 0.8 mm. The UV and IR transmission spectra have allowed us to obtain data on the content of impurities (nitrogen and hydrogen atoms) in samples. We have also analysed their correlation with the measured absorption coefficients, which were 0.057 – 0.53 cm^{-1}. For the thermal conductivity coefficient 1800 – 2200 W mK^{-1}, a high quality CVD diamond is suitable for producing output windows for high-power cw CO_2 lasers with a drastically decreased thermal lens effect.

Acknowledgements. The authors thank S.V. Voronin for participation in growing CVD diamond samples, I.I. Vlasov for the analysis of the samples by the Raman spectroscopy methods, R.A. Khmel'nitskii and G.V. Sharonov for providing us with single-crystal diamond samples. This work was supported by Federal Agency on Science and Innovations of the Russian Federation (State Contract No 02.523.12.3010).

References

1. Brierley C.J., Beck C.M., Kennedy G.R., Metcalfe J., Wheatley D. *Diamond Relat. Mater.*, **8**, 1759 (1999).
2. Pickles C.S.J., Madgwick T.D., Sussmann R.S., Wort C.J.H. *Diamond Relat. Mater.*, **9**, 916 (2000).
3. Thumm M. *Diamond Relat. Mater.*, **10**, 1692 (2001).
4. Savage J.A., Wort C.J.H., Pickles C.S.J., Sussmann R.S., Sweeney C.G., McClymont M.R., Brandon J.R. *Proc. SPIE Int. Soc. Opt. Eng.*, **3060**, 144 (1997).
5. Kaminskii A.A., Ralchenko V.G., Konov V.I. *Laser Phys. Lett.*, **3**, 171 (2006).
6. Thomas M.E. *Proc. SPIE Int. Soc. Opt. Eng.*, **2286**, 152 (1994).
7. Harris K., Herrit G.L., Johnson C.J., Rummel S.P., Scatena D. *Appl. Opt.*, **30**, 5015 (1991).
8. Pickles C.S.J., Madgwick T.D., Sussmann R.S., Wort C.J.H. *Diamond Relat. Mater.*, **9**, 916 (2000).
9. Dougls-Hamilton D.H., Hoag E.D., Seitz J.R.M. *J. Opt. Soc. Am.*, **64**, 36 (1974).
10. Sussmann R.S., Brandon J.R., Coe S.E., Pickles C.S.J., Sweeney C.G., Wasenczuk A., Wort C.J.H., Dodge C.N. *Industrial Diamond Rev.*, **58**, 69 (1998).
11. Dischler B., Wild C. (Eds). *Low-Pressure Synthetic Diamond: Manufacturing and Applications* (Berlin: Springer, 1998).
12. Ral'chenko V., Konov V. *Elektronika: Nauka, tekhnologiya, biznes*, (4), 58 (2007).
13. Masari M., Union P., Scarsbrook G.A., Sussmann R.S., Muys P. *Proc. SPIE Int. Soc. Opt. Eng.*, **2714**, 177 (1995).
14. Woerner E., Wild C., Mueller-Sebert W., Locher R., Koidl P., in: *Diamond Films, 9th CIMTEC'98 – Forum on New Materials, Symp. IV*, P. Vincenzini (Ed.) (Italy, Faenza: Techna Srl, 1999) p. 305.
15. Hass M., Davisson J.W., Kleyn P.H., Boyer L.L. *J. Appl. Phys.*, **45**, 3959 (1974).
16. Plotnichenko V.G., Sysoev V.K., Firsov I.G. *Zh. Tekhn. Fiz.*, **51**, 1903 (1981).
17. Tam A.C. *Rev. Mod. Phys.*, **58**, 381 (1986).
18. Rosencwaig A., in *Progress in Photothermal and Photoacoustic Science and Technology* (Prentice-Hall, Englewood Cliffs, NJ, 1994) Vol. 2, p. 73.
19. Brazhnik P.K., Novikov M.A. *Opt. Spektrosk.*, **70**, 453 (1991).
20. Glazov A.L., Muratikov K.L. *Zh. Tekhn. Fiz.*, **61** (11), 187 (1991).
21. Luk'yanov A.Yu., Novikov M.A. *Zh. Tekhn. Fiz.*, **70** (11), 99 (2000).
22. Brazhnik P.K., Novikov M.A., Pushkin A.A. *Opt. Spektrosk.*, **68**, 631 (1990).
23. Faubel W., Seidel B.S., Asche H.J. *Opt. Eng.*, **35**, 3555 (1996).
24. Francon M., Mallick S. *Polarization Interferometers: Application in Microscopy and Macroscopy* (NY: Acad. Press, 1971).
25. Luk'yanov A.Yu., Vladykin G.B., Aratskova A.A., Novikov M.A., Yashin Ya.I. *Zh. Fiz. Khim.*, **71**, 1497 (1997).
26. Antipov O.L., Kuzhelev A.S., Luk'yanov A.Yu., Zinov'ev A.P. *Kvantovaya Elektron.*, **25**, 891 (1998) [*Quantum Electron.*, **28**, 867 (1998)].
27. Klapshina L.G. et al. *New J. Chem.*, **30**, 616 (2006).
28. Podesta A., Salerno M., Ralchenko V., Bruzzi M., Sciortino S., Khmelnitskii R., Milani P. *Diamond Relat. Mater.*, **15**, 1292 (2006).
29. Nistor S.V., Stefan M., Ralchenko V., Khomich A., Schoemaker D. *J. Appl. Phys.*, **87**, 8741 (2000).
30. Clark C.D., Davey S.T. *J. Phys. C.: Sol. State Phys.*, **17**, 1127 (1984).

31. Zaitsev A.M. *Optical Properties of Diamond: a Data Handbook* (Berlin: Springer, 2001).
32. Kiflawi I., Welbourn C.M., Woods G.S. *Sol. State Commun.*, **85**, 551 (1993).
33. Plekhanov V.I., Luk'yanov A.Yu., Novikov M.A. *Pis'ma Zh. Tekhn. Fiz.*, **18** (2), 57 (1992).
34. Masseti E., Montecchi M., Da Silva M.P. *Thin Sol. Films*, **234**, 557 (1993).
35. Luk'yanov A.Yu., Pogorelko A.A. *Zh. Tekhn. Fiz.*, **72** (5), 72 (2002).
36. Luk'yanov A.Yu., Tyukaev R.V., Pogorelko A.A., Pereskokov A.A., Gavrishchuk E.M. *Opt. Spektrosk.*, **94**, 41 (2003).
37. Sukhadolau A.V., Ivakin E.V., Ralchenko V.G., Khomich A.V., Vlasov A.V., Popovich A.F. *Diamond Relat. Mater.*, **14**, 589 (2005).
38. Harris D.C. *Proc. SPIE Int. Soc. Opt. Eng.*, **2286**, 218 (1994).
39. Burns R.C., Cvetkovic V., Dodge C.N., Evans D.J.F., Rooney M.L.T, Spear P.M., Welbourn C.M. *J. Cryst. Growth.*, **104**, 257 (1990).
40. Inyushkin A.V., Ral'chenko V.G., Taldenkov A.N., Artyukhov A.A., et al. *Kr. Soobshch. FIAN*, (11), 36 (2007).